Lehrstuhl für Bildverarbeitung
Institute of Imaging & Computer Vision

Digital Radiography Enhancement by Nonlinear Multiscale Processing

Martin Stahl and Til Aach and Sabine Dippel

in: Medical Physics. See also BIBTEX entry below.

BIBTEX:

```
@article{STA00a,
author = {Martin Stahl and Til Aach and Sabine Dippel},
title = {Digital Radiography Enhancement by Nonlinear Multiscale
   Processing},
journal = {Medical Physics},
volume = {27},
number = {1},
year = {2000},
pages = {56--65}}
```


document created on: December 19, 2006
created from file: MedPhys00coverpage.tex
cover page automatically created with CoverPage.sty
(available at your favourite CTAN mirror)

RWTH AACHEN
RHEINISCH-WESTFÄLISCHE TECHNISCHE HOCHSCHULE AACHEN

Digital radiography enhancement by nonlinear multiscale processing

Martin Stahl
Philips Research, Roentgenstrasse 24-26, D-22335 Hamburg, Germany

Til Aach
Medical University of Lübeck, Ratzeburger Allee 160, D-23538 Lübeck, Germany

Sabine Dippel
Philips Research, Roentgenstrasse 24-26, D-22335 Hamburg, Germany

(Received 16 December 1998; accepted for publication 15 October 1999)

Today's digital radiography systems mostly use unsharp maskinglike enhancement algorithms based on splitting input images into two or three frequency channels. This method allows fine detail enhancement as well as processing of global contrast (harmonization). However, structures of medium size are not accessible. In extension of a standard algorithm of such type, we develop and test a new enhancement algorithm based on hierarchically repeated unsharp masking, resulting in a multiscale architecture allowing consistent access to structures of all sizes. Our algorithm decomposes a radiograph by a pyramid-architecture, dividing it into eight or more channels representing structures of different sizes, known as "scales." At each scale, weakly contrasting structures are then enhanced by suitable nonlinear processing. We emphasize two points: first, backward compatibility to the standard algorithm which is used routinely in clinical practice. This allows reuse of current parametrization know-how as well as a smooth transition from current to new processing. Second, our enhancement is noise-resistant in the sense that it prevents unacceptable noise amplification. A prototype implementation of the algorithm is undergoing trials in the clinical routine of radiology departments of major German hospitals. Results strongly indicate the superior performance and high acceptance of the new processing. © *2000 American Association of Physicists in Medicine.* [S0094-2405(00)01401-2]

Key words: digital radiography, image enhancement, multiresolution techniques, multiscale enhancement, noise resistance

I. INTRODUCTION

Radiographs often contain large variations of radiographic density together with detail information of only very weak contrast. For instance, in a chest image mediastinum and thoracic spine absorb strongly, while the lungs are almost x-ray transparent. A similar situation occurs when imaging metal implants, like artificial hip joints, which exhibit a very large x-ray attenuation relative to surrounding tissue. Hard- or softcopy display of such images then often faces the dilemma of having to reproduce these large variations without clipping, while at the same time subtle details, like lung nodules, must remain visible.

In digital radiography, these conflicting requirements can be reconciled by suitable digital processing before image display, e.g., on film or on a monitor.[1–3] Most present systems separate the image into two (or three) frequency bands.[4,5] As the large intensity variations occur predominantly over low spatial frequencies, information in the low-frequency channel is attenuated relative to higher spatial frequencies (harmonization, dynamic range equalization).[2,6] Subtle details then occupy relatively larger portions of the available dynamic range, hence making them better visible. A potential third channel contains very high spatial frequencies, allowing edge sharpening or noise reduction.[5–7] Receiver operating characteristic (ROC) studies show that detail perception can indeed be improved by appropriate processing.[1]

While these image enhancement methods have been tuned towards considerable performance over the years, improved image decomposition techniques, like wavelets[8] and pyramids,[9,10] have emerged. These *multiscale* techniques decompose images into several frequency channels. The advantage of these decomposition techniques is that structures of different size appear separately in different scales, and can be processed independently. This concept was applied to television images in Ref. 11, where the Laplacian pyramid[9] was used for decomposition. Coefficients on each scale were then subjected to an odd nonlinear enhancement function. Applications of this concept to clinical radiographs are described, for instance, in Ref. 12 and 13. In Ref. 12, the input images are decomposed by a redundant dyadic wavelet transform (RDWT). Wavelet coefficients are enhanced by an odd nonlinear and monotonically increasing enhancement function, which is made up of piecewise linear functions. The prime application area of the algorithm is mammography. In Ref. 13, scales are generated by the Laplacian pyramid in the same manner as in Ref. 11. (Note that Fan and Laine in Ref. 12 also selected a Laplacian filter rather than a gradient-type filter to use in the RDWT of their algorithm.) As in Ref. 11, a nonlinearity is applied toward the end of equalizing detail amplitude at each scale in radiographs, achieving appreciable results.

However, when applied to (digital) radiographs, we found

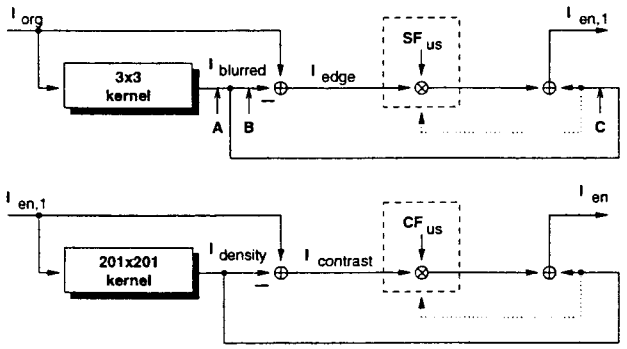

FIG. 1. Two-step unsharp-masking-based processing.

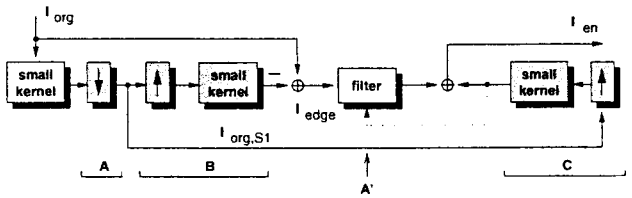

FIG. 2. Modified unsharp-masking.

that these approaches are similarly sensitive to noise as unsharp masking-based algorithms. The reason for this is that the finest scale is more or less equivalent to the high-frequency channel of the described standard processing (cf. Refs. 12 and 14), where noise is most critical.

A prominent issue in the development of our algorithm therefore is robustness against noise. To avoid loss of weakly contrasting detail information, we have refrained from integrating genuine denoising into our approach, as is done in, e.g., Ref. 12, by wavelet coefficient shrinkage. Instead, we seek to prevent unacceptable noise amplification during image enhancement. Special attention was paid to this point when designing the enhancement function and the processing strategy for the finest scales.

Another important issue is that we have developed our algorithm as an extension of a linear unsharp masking algorithm for harmonization and edge enhancement, which is used routinely in clinical practice. In particular, our algorithm is almost fully backwards compatible. This was achieved by regarding multiscale processing as hierarchically repeated unsharp masking, and mapping the existing algorithm on a multiscale structure. This is convenient for two reasons: first, parameters of the unsharp masking algorithm have direct counterparts in the new processing. This allows reuse of the parametrization know-how accumulated over the years in a radiology department. Second, it enables a smooth transition from the current algorithm to the new processing, rather than confronting radiologists with a completely new appearance of their images.

In the following, we first describe how our multiscale algorithm evolves from the linear unsharp masking algorithm. We then design the nonlinear enhancement function. Then, the method used to contain noise is developed. Before concluding, we give details of a clinical setup of our algorithm and some preliminary results of an ongoing clinical application.

II. FROM UNSHARP MASKING TO MULTISCALE PROCESSING

We start with the following reference algorithm, which is used routinely in storage phosphor systems.[6] As shown in Fig. 1, the algorithm consists of two steps. First, a slightly blurred version I_{blurred} is generated from the input image I_{org} by convolution with a small box kernel of size 3×3 pixels, which is then subtracted from the original. The resulting high-frequency image I_{edge} contains mostly edge information, and is enhanced by a constant *sharpness factor* SF_{us}. Adding the enhanced highpass data to I_{blurred} results in a processing result with increased perceived sharpness (*edge enhancement*). In the second step, a large box kernel–e.g., 201×201 pixels for a $2k\times2k$-radiograph—is applied to separate middle and high spatial frequencies (contrast information, I_{contrast}) from the very low ones. Subjecting I_{contrast} to a contrast factor CF_{us} amplifies contrast information relative to the large and low-frequency density variations I_{density} (*harmonization*). Note that nonlinear amplification as in Ref. 7 is easily introduced into this structure by density- or contrast-dependent gain factors (see dotted lines in Fig. 1).

When one intends to enhance primarily low contrast by a nonlinear gain, this algorithm obviously allows separate access only to fine detail and low-frequency information. Medium-sized structures remain grouped together in I_{contrast}, which comprises a broad frequency band. To exploit the full potential of nonlinear processing for structures of arbitrary size, it is required to split up this frequency band further. For convenience, we seek to hierarchically continue the edge enhancement operation, where, to avoid an impractical increase in the amount of data, each filtered image is subsampled. Subsampling leads to the following modifications marked A, B, and C in Fig. 2:

(i) A: The lowpass image I_{blurred} is subsampled by a factor of 2 in each direction (↓).

(ii) B,C: For subtraction from the original image as well as addition in the reconstruction path, this image is expanded again, i.e. zeros are inserted between the available samples (↑) followed by another low pass.

Ideally, the low pass preceding the subsampling should cut off at half the Nyquist frequency. For practical reasons, only small filter kernels—like 3×3 or 5×5 binomial kernels—are used, thus introducing some aliasing into the subsampled images. Since aliasing cancels out during reconstruction, this is not critical. This balance between produced and cancelled aliasing is disturbed by subband processing but generally not to a severe degree.

Subsampling generates an image $I_{\text{org},S1}$ of half-size in each dimension, representing the spatial frequencies up to half the Nyquist frequency of the original image. The image itself, however, contains spatial frequencies up to the original Nyquist frequency, because subsampling has doubled all actually present frequencies. $I_{\text{org},S1}$ thus is a sharp but

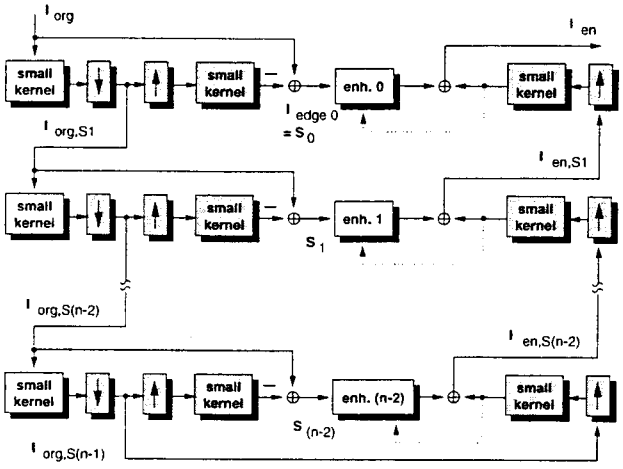

FIG. 3. The Laplacian pyramid with subband enhancement filters.

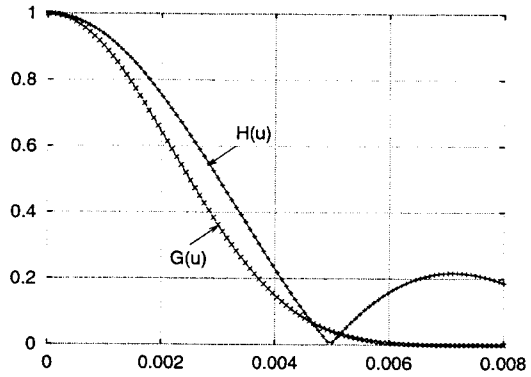

FIG. 4. Comparison of the modulus spectrum $|H(u)|$ of a one-dimensional box kernel to a pyramid transfer function $G(u)$ considering only the low-pass level. The length of the box kernel is $N=201$ pixels. The pyramid consists of eight levels, each using a binomial kernel with a length of 3 pixels.

smaller image, the edges of which correspond to larger structures in the original. Therefore, the same filter as already used in Fig. 2 can be utilized at A' to process $I_{\text{org},S1}$. Repeating this nesting of unsharp-masking operations n times leads to the decomposition in Fig. 3, known as the Laplacian pyramid.[9] Subsampling serves the double purpose of avoiding unnecessary increase of the amount of data, and allowing the use of the same small low-pass kernel throughout all levels of the pyramid. In the following, the difference images will be referred to as subband images, subbands, or scales.

For backward compatibility, the reference algorithm is easily mapped to the pyramid. Using 3×3 binomial filter kernels at each pyramid level, the finest, uppermost level of the pyramid I_{edge0} is almost equivalent to the edge image I_{edge} of Fig. 1. The number of pyramid levels needed is determined by requiring the (expanded) low-pass level generated within the pyramid to be approximately equivalent to I_{density} in Fig. 1. The transfer function of the pyramid to the low-pass level should hence approximate the spectrum of the large box kernel. The spectrum $H(u)$ of a box kernel filter of length N is given by

$$H(u)=\frac{1}{N}\cdot\frac{\sin(N\cdot\pi\cdot u)}{\sin(\pi\cdot u)}. \tag{1}$$

The low-pass filter chosen for the pyramid is a separable binomial filter of size 3×3 pixels, based on the one-dimensional kernel [0.25, 0.5 0.25]. Its spectrum $G_L(u)$ is given by

$$G_L(u)=(\cos(\pi\cdot u))^2. \tag{2}$$

Applying this kernel recursively in an n-level pyramid including frequency doubling caused by subsampling yields the transfer function to the low-pass level of the pyramid. To obtain the transfer function for the expanded low-pass level, $G_L(u)$ must be squared since pyramid reconstruction applies the same sequence of filters again, yielding

$$G(u)=\left(\prod_{i=0}^{n-2} G_L(2^i\cdot u)\right)^2. \tag{3}$$

Aliasing was neglected throughout to simplify the calculation. As Fig. 4 shows, the spectrum of a box kernel of size $N=201$ can be approximated by a pyramid consisting of eight levels.

Mapping of the linear filtering operations shown in Fig. 1 is now easily done by applying the following constant factors CF_i to the subband images:

$$CF_0=SF_{us}\cdot CF_{us},$$
$$CF_i=CF_{us} \quad \text{for } 0<i<n-2. \tag{4}$$

The low-pass subband image remains unchanged. Unsharp masking algorithms with density- or contrast-dependent nonlinear gain are mapped similarly by applying the gain characteristics to the corresponding pyramid levels.

Note that a similar relation between unsharp masking and RDWT linear enhancement is discussed in Ref. 12, where, however, it was not necessary to consider subsampling. As the number n of levels needed here turns out to be rather large ($n=8$), RDWT is impractical since it would increase the data volume by a factor of 7, whereas the Laplacian pyramid generates an increase of less than a third. This point is of particular importance with respect to the forthcoming introduction of solid state detectors[15] capable of acquiring images up to $3k\times3k$ pixels.

III. THE ENHANCEMENT FUNCTION

A. Enhancement in noise

The purpose of the enhancement function is to amplify weak subband coefficients c in each subband i more than stronger ones, regardless of their sign. It will hence be nonlinear, odd, and monotonically increasing, but with decreasing slope as $|c|$ gets large. Denoting the enhanced subband coefficients by $\hat{c}$, the enhancement operation can be written as $\hat{c}=L_i(c)$, where $L_i(c)$ is the enhancement function, or, in terms of an amplification $CF_i(c)$, as

$$\hat{c}=CF_i(c)\cdot c. \tag{5}$$

As the aim is to enhance contrast rather than density, this type of enhancement is applied to the high-pass level and all bandpass levels of the pyramid, but not to the low-pass level.

The enhancement function $L_i(c)$ and hence also the amplification $\mathrm{CF}_i(c)$ are often a composite of two or more functions defined over adjacent intervals of c, with $L_i(c)$ respectively $\mathrm{CF}_i(c)$ being continuous but only piecewise differentiable.[12,13] We argue here that especially to reduce undesired amplification of noise for any given operating point on the enhancement function, $\mathrm{CF}_i(c)$ should be free of steep slopes and bends.[16,17] In Refs. 16 and 17, it is shown that this type of noise amplification can be kept low if a smooth amplification function is chosen, the derivative of which does not take too large values. For the same reason, we decided against genuine denoising by shrinking small coefficients, since the necessary transition from amplification to attenuation implies a rather steep slope. We therefore use an amplification function which is differentiable for all $c \neq 0$, since this ensures linear amplification of infinitesimal coefficient fluctuations at each operating point.

In addition to these considerations, we have sought to separately control amplification of subband coefficients c close to zero, which often—but not always—represent noise only.

B. The gain function (structure boost)

When combining the above considerations with the requirement of backward compatibility, the contrast amplification function—in the following also termed *structure boost*—should meet the following criteria:

(i) For large contrasts the function should have a constant value CF_i according to (4).

(ii) For contrast values close to zero the function should approach $\mathrm{CF}_i + G_i$, $G_i \geq 0$. G_i defines the additional gain for weak contrasts within subband image i. For $G_i = 0$, $0 \leq i \leq n-2$, structure boost is disabled and our algorithm behaves like linear unsharp-masking in Fig. 1.

(iii) The function should be smooth everywhere, especially for small contrast values c.

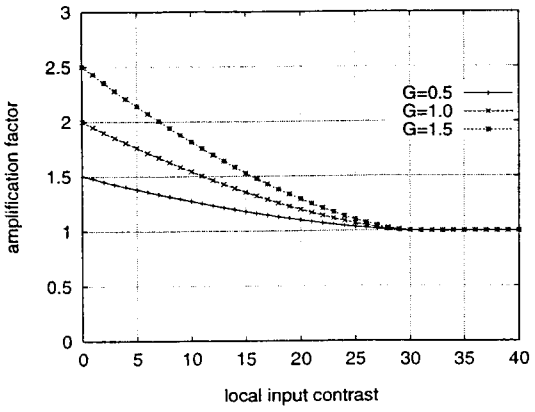

FIG. 5. Contrast amplification function according to (6) for $c_0 = 30$, $p = 1.5$, $\mathrm{CF}_i = 1.0$, and various values of G.

An amplification function complying with these criteria is given by

$$\mathrm{CF}_i(c) = \begin{cases} G_i \cdot \left(1 - \dfrac{|c|}{c_0}\right)^{p_i} + \mathrm{CF}_i & \text{for } |c| \leq c_0, \\ \mathrm{CF}_i & \text{else,} \end{cases} \tag{6}$$

which is shown in Fig. 5 for several values of G_i. The enhancement in addition to the linear factor CF_i is restricted to contrasts between zero and the transition amplitude c_0. $\mathrm{CF}_i(c)$ is differentiable for all $c \neq 0$, including $c = \pm c_0$. The gain G_i allows a smooth transition towards the linear unsharp-masking processing. The exponent p defines how fast the amplification decreases towards CF_i for increasing $|c|$. As desired, p does not influence the amplification of contrast values close to zero which is determined by G_i. It can therefore be used to control the amount of weak structure enhancement while being to some extent robust against noise amplification. As it turned out during clinical evaluations, making G and p adjustable is of practical use, whereas for the transition amplitude c_0 a constant value can be chosen, which depends only on type of imaging system used.

IV. NOISE CONTAINMENT

A. The noise problem

Noise in radiographs stems from a variety of sources, including quantum noise, structure noise of the detector, light photon shot noise, electrical noise, and quantization noise.[3,18,19] The noise power spectrum (NPS) depends on the incident x-ray dose and on spatial frequency. Quantum noise, for instance, is Poisson distributed and low-pass filtered by the imaging system's modulation transfer function (MTF).[3,19–21] With respect to our enhancement algorithm, the following effects are of major concern: first, the distribution of the total noise power over the scales is determined by both NPS and bandwidth of the scales. Since the pyramid divides both spatial frequency axes into octaves, the finest scale $i = 0$ represents about three-quarters of the original spectral bandwidth, scale $i = 1$ about 3/16, and so on. Due to their large bandwidths, most of the noise power will hence be found in the finest scales, despite the drop-off of the NPS over higher spatial frequencies. Second, the Poissonian na-

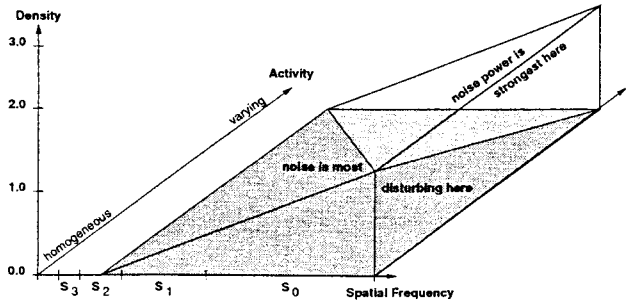

FIG. 6. Qualitative plot of subjective noise visibility dependent on signal activity taking into account physical presence of noise. The spatial frequency is subdivided into n octaves according to the subband images S_0, S_1, ..., S_{n-2}, $I_{S(n-1)}$.

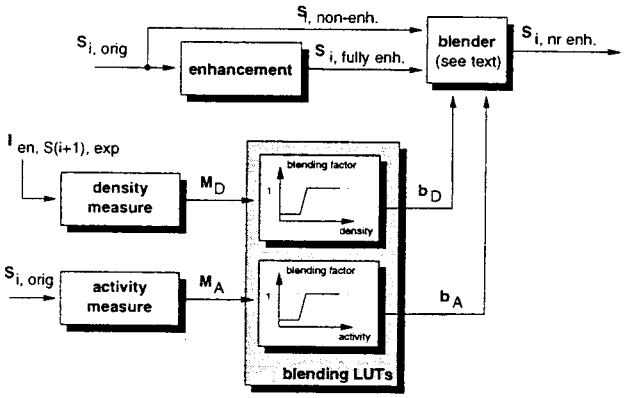

FIG. 7. Blockdiagram of the noise containment algorithm.

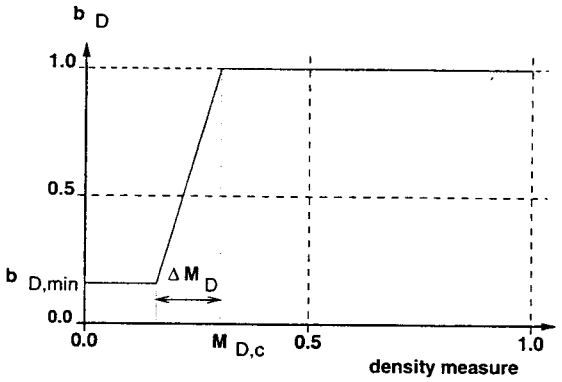

FIG. 8. Weighting factor b_D for noise containment as function of the local density measure M_D.

ture of quantum noise implies that noise variance is higher in regions with higher incident x-ray dose. Subsequent nonlinear processing stages profoundly alter this signal dependence. In the mentioned SPS imaging system, the detected images are subjected to a logarithmic gain curve and their intensities inverted.[18,19,21] The overall result is that noise power is strongest in regions of low optical density, which are displayed as bright regions. Noise hence affects our enhancement algorithm predominantly in those regions of the finest scales which correspond to low optical density.

Subjectively, noise is most strongly visible in areas of weak or no texture-caused intensity fluctuations ("activity"). These results are qualitatively summarized in Fig. 6. In the next section, we discuss a noise containment strategy which keeps noise amplification within acceptable limits without losing the benefits of weak structure enhancement.

1. Realization of noise containment

The basic idea to noise containment is to apply less enhancement to noise-sensitive regions of the parameter space, viz. to areas in the finest subbands corresponding to low optical density and activity. A convenient way of implementation is to first fully enhance each subband image, and then to gradually blend in the unprocessed subband before the entire radiograph is reconstructed. The degree b of blend-in depends on the subband index i (which corresponds to spatial frequency), local image density, and local activity. A block diagram of the algorithm is given in Fig. 7. The enhanced subband $S_{i,\text{fully enh}}$ and the original subband $S_{i,\text{orig}}$ are weighted and added according to

$$S_{i,\text{nr enh}}(x,y) = b_D(x,y)\cdot b_A(x,y)\cdot S_{i,\text{fully enh}}(x,y) + (1 - b_D(x,y)\cdot b_A(x,y))\cdot S_{i,\text{orig}}(x,y), \quad (7)$$

providing a noise robust pixel value $S_{i,\text{nr enh}}(x,y)$. The density- and activity-dependent factors $b_A(x,y)$ and $b_D(x,y)$ determine the weight of the enhanced subband in (7).

The described method is easy to implement and the concept works regardless of the type (linear, nonlinear, ...) of the enhancement filter. In addition, it is easily adapted when the properties of noise change, for instance when using a differ-

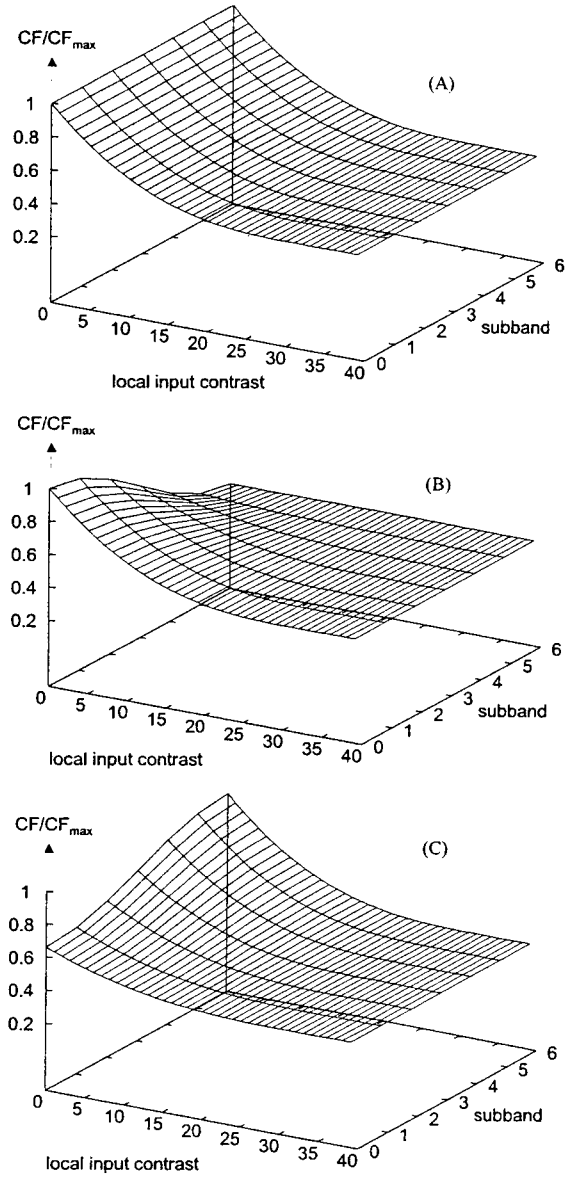

FIG. 9. Suband-dependent contrast amplification: no specific frequencies preferred (a), high frequencies preferred (b), low frequencies preferred (c).

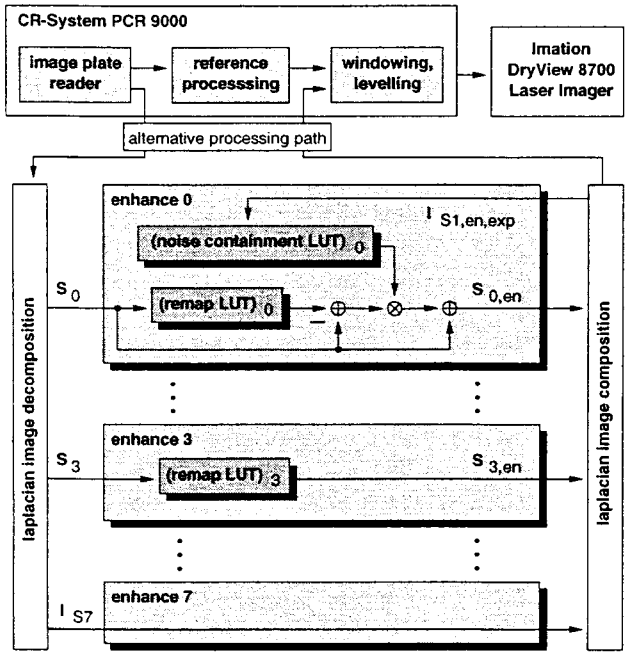

FIG. 10. Clinical prototype linked to PCR 9000 CR system.

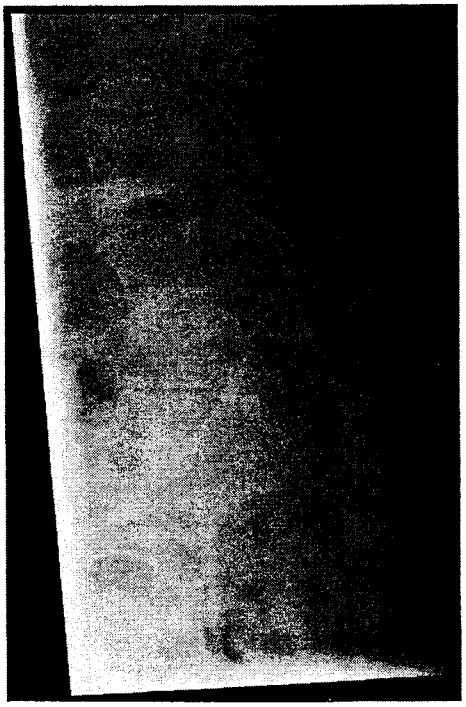

FIG. 11. Sacrum processed with standard unsharp-masking algorithm.

ent type of acquisition system. Most important, a subband coefficient is never attenuated below its original, unprocessed value.

The local density measure M_D can easily be retrieved from the expanded and enhanced image of the next lower level of the pyramid $I_{\mathrm{en},S(i+1)\mathrm{exp}}$. Similarly, a local activity measure M_A can be calculated within each subband, e.g., by standard deviation, local entropy, or similar measures. An example of b_D versus M_D is given in Fig. 8. The density-dependent weighting factor b_D is one in dark areas (high optical density), corresponding to full contrast enhancement. Starting at a critical density value $M_{D,c}$ it decreases over the interval ΔM_D towards a value $b_{D,\min}$ corresponding to a residual enhancement. This transition, however, depends on the subband: whereas in high-frequency subbands for low densities a reduction of enhancement might be necessary, it will not be needed in lower-frequency subbands with better signal-to-noise ratios. For b_A versus M_A similar considerations hold. Activity measures can be calculated using, for instance, the standard deviation or one-dimensional histogram-based measures like information (negative entropy) or energy.

B. Equalization

From a technical point of view, equal treatment of all subbands in nonlinear multiscale processing provides excellent detail representation without preferring any specific spatial frequencies. Therefore, one might expect that this processing, unlike unsharp masking,[6,22] does not need any examination specific parametrization.[13] On the other hand, the splitting of the image into subbands provides the option of a subtle differentiation between the processing of specific subbands, in the following denoted as *equalization*. On closer examination it becomes obvious that equalization could be beneficial from a diagnostic point of view:

(i) **Adaptation of processing to diagnostic interest**: In many cases only details of a certain size are of diagnostic interest. In such cases too much superimposing

TABLE I. Processing parameters of standard processing ($CF_{us}=1.5$, $SF_{us}=2.2$, small box kernel of size 3×3 pixels, large box kernel of size 201×201 pixels) for sacrum image mapped to multiscale processing according to Eq. (4) and Fig. 4. Spatial resolution: 5 pixel/mm, pyramid kernel: 3×3 binomial, number of subbands: 8. For gain $G=0$, the exponent p has no effect ("undefined").

Subband	0	1	2	3	4	5	6
CF	3.3	1.5	1.5	1.5	1.5	1.5	1.5
p	undefined	undefined	undefined	undefined	undefined	undefined	undefined
G	0.0	0.0	0.0	0.0	0.0	0.0	0.0
c_0	0.0	0.0	0.0	0.0	0.0	0.0	0.0
$M_{D,c}$	0.0	0.0	0.0	0.0	0.0	0.0	0.0
ΔM_D	0.0	0.0	0.0	0.0	0.0	0.0	0.0
$b_{D,\min}$	1.0	1.0	1.0	1.0	1.0	1.0	1.0

TABLE II. Multiscale processing parameters for sacrum image. Spatial resolution: 5 pixel/mm, pyramid kernel: 3×3 binomial, number of subbands: 8.

Subband	0	1	2	3	4	5	6
CF	1.5	1.5	1.5	1.5	1.5	1.5	1.5
p	2.1	2.1	2.1	1.2	1.2	1.2	1.2
G	1.0	1.0	1.0	1.3	1.3	1.3	1.3
c_0	30	30	30	30	30	30	30
$M_{D,c}$	0.4	0.4	0.4	0.0	0.0	0.0	0.0
ΔM_D	0.14	0.14	0.14	0.0	0.0	0.0	0.0
$b_{D,\min}$	0.5	0.5	0.5	1.0	1.0	1.0	1.0

detail information could hamper the diagnostic process. Equalization can reduce disturbing superpositions of diagnostically relevant details by nonrelevant details.

(ii) **Adaptation of processing to actual information content of the image**: Detail information is not distributed equally over all subbands for all examinations. For some examinations certain subbands hardly contribute. Enhancement of these subbands only carries the risk of enhancing noise.

(iii) **Subjective improvement of image quality**. Equalization allows modification of the global impression of the image without necessarily affecting the visibility of details. Our clinical experiences show that, for many examinations, the preferred processing result could not be achieved with equal treatment of all subbands. This taste aspect may have some relevance for the acceptance of the processing algorithm.

The most prominent effect can be achieved by a subband-dependent modification of the linear factor CF. However, this implies the risk of producing artifacts: preference of high frequencies could produce overshoots at steep edges,[2] suppression of very low frequencies could reverse the density gradient[13] and therefore distort diagnostically relevant information. Applying the equalization only to the structure boost part of function (6) allows the above-mentioned requirements to be met without producing visible artifacts. Through the gain factor G_i the effects of noise in the different subbands can be directly taken into account, namely by reducing noise amplification in subbands without relevant detail information. Figure 9 shows three subband-dependent plots of the contrast amplification functions which we determined during clinical trials as most relevant:

FIG. 12. Sacrum processed with multiscale algorithm.

(a) Equal treatment of all subbands seems adequate for images where the diagnostic interest is equally distributed from very small to large details. Superposition effects should not be reduced but structures of different sizes should become easier to distinguish. Boosting of the noise level may irritate in some regions of the image. In this case the noise compensation mechanism proved to be a suitable countermeasure. Typical examples are lateral spine images.

(b) Preference of higher spatial frequencies provides a sharper image impression. This seems adequate for images where the diagnostic interest is mainly in small details like bone texture. Stronger enhancement of lower frequencies increases distracting density variations resulting from superposed soft tissue. This holds for examinations of the extremities, especially for hands and feet. Some boosting of noise was accepted because noise is masked by high-frequency texture information.

(c) Preference of lower spatial frequencies seems adequate for many examinations of the trunk (e.g., pelvis, abdomen), where the images contain few small sized details of diagnostic interest. This type of enhancement is a good means to prevent too much noise amplification (see Fig. 6). Clinicians judged this to give a three-dimensional impression to the images. Pelvis images, for instance, were found to look similar to conventional (analog) radiographs without losing the advantage of better exploitation of the available dynamic range.

TABLE III. Multiscale processing parameters for lateral dorsal spine. Spatial resolution: 5 pixel/mm, pyramid kernel: 3×3 binomial, number of subbands: 8.

Subband	0	1	2	3	4	5	6
CF	1.1	1.1	1.1	1.1	1.1	1.1	1.1
p	3.0	3.0	3.0	3.0	3.0	3.0	3.0
G	1.0	1.0	1.0	1.3	1.3	1.3	1.3
c_0	30	30	30	30	30	30	30
$M_{D,c}$	0.35	0.35	0.35	0.0	0.0	0.0	0.0
ΔM_D	0.14	0.14	0.14	0.0	0.0	0.0	0.0
$b_{D,\min}$	0.0	0.0	0.0	1.0	1.0	1.0	1.0

V. CLINICAL APPLICATION

A. Clinical example implementation

The multiscale algorithm was implemented on a clinical prototype linked to a PCR 9000 computed radiography system, as depicted in Fig. 10. PCR 9000 standard processing, described in Sec. II, is bypassed by a module performing the nonlinear multiscale processing. Image acquisition (PCR 9000 image plate reader) including preranging of the images, determination of printer gray-scale look-up table, as well as the HCU (Imation DryView 8700 Laser Imager) are shared by both types of processing, allowing a direct comparison of old and new processing.

The multiscale processing consists of a nonlinear contrast remapping operation according to (6), individually parametrized for each subband image. For the three uppermost subbands noise containment (see Sec. IV) was implemented, where only the density-dependent part was included. During our clinical trials we sought to optimize the parametrization of the multiscale processing according to the comments of experienced radiologists. Parametrization of the standard processing was considered as being optimized through years of routine clinical use. Two representative results are given in the following:

B. Sacrum, lateral view

The unprocessed image exhibits very poor contrast and low signal to noise ratio, caused in part by disturbing superpositions of the pelvis and soft tissue. Standard processing improves the image impression only marginally, and is noticably limited by noise (Fig. 11). The processing parameters can be found in Table I. The parameters for the multiscale processing after optimization are given in Table II. Radiologists said multiscale processing provides an improved detail representation, e.g., bone contour representation, without disturbing boost of noise (Fig. 12). The preferred enhancement of the larger details was selected, because few small-sized details of diagnostic interest can be found in the image. Stronger enhancement of fine scales would only boost the noise level without bringing more detail information into the image.

C. Dorsal spine, lateral view

A good representation of all regions must cope with large density variations between the medium region and the upper and lower boundary areas. In the upper boundary area the shoulder blades cause disturbing superpositions, while in the lower boundary area the large density transition between lung and abdominal cavity must be handled. In both boundary areas, high noise levels degrade the image impression. Additionally, superpositions of bodies of vertebrae by ribs and pulmonary vessels hamper diagnosis. The parameters for the multiscale processing are given in Table III. Radiologists said multiscale processing facilitates to distinguish vertebrae from superimposing structures, such as pulmonary vessels. Equal treatment of all scales is appropriate because diagnos-

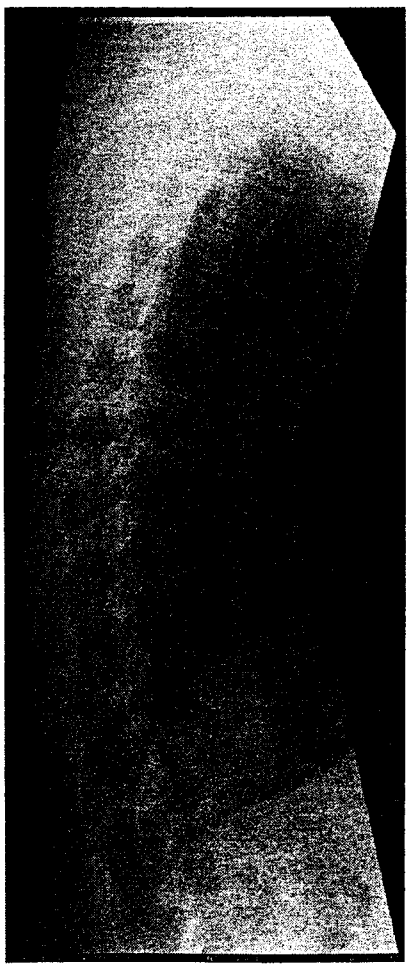

FIG. 13. Dorsal spine processed with multiscale algorithm with noise containment.

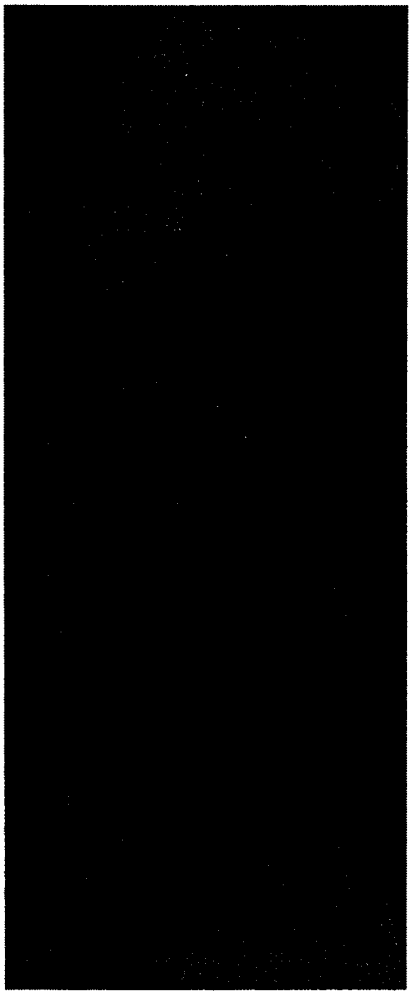

FIG. 14. Pixelwise difference image (contrast stretched) between dorsal spine images processed with and without noise containment, i.e., critical density $M_{D,c}=0$ for all subbands. Evidently, noise containment reduces noise boosting in image areas near the upper and lower image edge, without compromising enhancement of other parts of the image.

tic interest targets small details, such as posterior edges of vertebrae, as well as larger details like bodies of vertebrae themselves. Unacceptable noise boosting on the finest scales, particularly in the bright regions of the upper and lower parts of this radiograph, could successfully be prevented through the noise containment feature (Figs. 13 and 14). More examples can be found in Ref. 23.

VI. CONCLUSIONS

We developed a new nonlinear multiscale algorithm that can be derived from unsharp masking-based standard processing. Backward compatibility enables reuse of processing know-how acquired on current standard processing and eases acceptance of the new algorithm. Particular attention was paid to noise robustness.

First clinical trials strongly indicate that a suitable design of the subband processing yields an improved detail visibility for a broad spectrum of routine radiographs without unacceptable boosting of noise. We note, however, that the achievable quality enhancement appears to depend on the type of examination. For some examinations like hand, results from standard processing were already close to optimum,[23] since no hidden details could be made better visible.

Detectors of the next generation as, e.g., solid state detectors, will bring further improvements with respect to versatility, signal-to-noise ratio, dynamic range, and spatial resolution.[3,15,24,25] These detectors are likely to encounter similar challenges in terms of image processing and rendering, so that we expect the algorithm described here to help exploit the full potential of these detectors.

ACKNOWLEDGMENTS

We thank the head, Professor J.-P. Haas, and staff of the radiology department of Fulda Municipal Hospital for their support. We are especially grateful to Dr. E. Müller for his helpful contributions and his patience during many extended sessions. We furthermore thank our colleagues at Philips Medical Systems, Hamburg, for fruitful discussions, technical help, and for providing applicational background.

[1] M. Ishida, "Image Processing," in *Computed Radiography*, edited by Y. Tateno, T. Iinuma, M. Takano (Springer Verlag, Berlin, 1987), pp. 25–30.
[2] A. R. Cowen, P. J. Hartley, and A. Workman, "The computer enhancement of digital gey-scale fluorography images," Br. J. Radiol. **61**, 492–500 (1988).
[3] T. Aach, U. Schiebel, and G. Spekowius, "Digital image acquisition and processing in medical x-ray imaging," J. Electron. Imaging **8**(1), 7–22 (Special Section on Biomedical Image Representation) (1999).
[4] I. Maack and U. Neitzel, "Optimised image processing for routine digital radiography," in *Proceedings Computer Assisted Radiology (CAR 91)*, edited by U. Lemke (Springer Verlag, Berlin, 1991), pp. 108–114.
[5] T. L. Ji, M. K. Sundareshan, and H. Roehrig, "Adaptive image contrast enhancement based on human visual properties," IEEE Trans. Med. Imaging **13**(4), 573–586 (1994).
[6] A. G. Davies, A. R. Cowen, G. J. S. Parkin, and R. F. Bury, "Optimising the processing and presentation of PPCR images," SPIE **2712**, 189–195 (1996).
[7] A. R. Cowen, A. Giles, A. G. Davies, and A. Workman, "An image processing algorithm for PPCR imaging," SPIE **1898**, 833–843 (1993).
[8] A. N. Akansu and R. A. Haddad, *Multiresolution Signal Decomposition* (Academic, Boston, 1992).
[9] P. J. Burt and E. H. Adelson, "The Laplacian pyramid as a compact image code," IEEE Trans. Commun. **31**(4), 532–540 (1983).
[10] E. H. Adelson, C. H. Anderson, J. R. Bergen, P. J. Burt, and J. M. Ogden, "Pyramid methods in image processing," RCA Engineer **19**(6), 33–41 (1984).
[11] R. F. Bessler and J. H. Arbeiter, "Contrast enhancement using Burt pyramid processing," in *SID International Symposium, Digest of Technical Papers*, San Diego, 6–8 May 1986, pp. 352–353.
[12] J. Fan and A. Laine, "Contrast Enhancement by Multiscale and Nonlinear Operators," in *Wavelets in Medicine and Biology*, edited by A. Aldroubi and M. Unser (CRC, Boca Raton, FL, 1996), pp. 163–189.
[13] P. Vuylsteke and E. Schoeters, "Multiscale image contrast amplification (MUSICA™)," SPIE **2167**, 551–560 (1994).
[14] A. F. Laine, J. Fan, and S. Schuler, "Discrete dyadic wavelet transform for contrast enhancement," SPIE **2303** (Wavelet Application in Signal and Image Processing), 456–460 (1994).
[15] N. Jung, P. L. Alving, F. Busse, N. Conrads, H. M. Meulenbrugge, W. Rütten, U. Schiebel, M. Weibrecht, and H. Wieczorek, "Dynamic x-ray imaging system based on an amorphous silicon thin-film array," SPIE **3336**, 396–407 (1998).
[16] T. Aach, "Spectral transform-based nonlinear restoration of medical images: Algorithms and a comparative evaluation," SPIE **3646** (Nonlinear Image Processing), 270–280 (1999).

[17] T. Aach and D. Kunz, "X-ray image restoration by spectral amplitude estimation as an extension of a speech enhancement approach," in *Proceedings 9. Aachener Symposium on Signal Theory*, edited by B. Hill, M. Junggeburth, and F. W. Vorhagen (Aachen, Germany, 1997), pp. 75–80.
[18] W. Hillen, U. Schiebel, and T. Zaengel. "Imaging performance of a digital storage phosphor system," Med. Phys. **14**, 744–751 (1987).
[19] E. Ogawa, S. Arakawa, M. Ishida, and H. Kato, "Quantitative analysis of imaging performance for computed radiography systems," SPIE (Medical Imaging 1995: Image Processing) **2432**, 421–431 (1995).
[20] M. Rabbani, R. Shaw, and R. van Metter, "Detective quantum efficiency of imaging systems with amplifying and scattering mechanisms," J. Opt. Soc. Am. A **4**(5), 895–901 (1987).
[21] S. M. Kengyelics, J. H. Launders, and A. R. Cowen, "Physical imaging performance of a compact computed radiography acquisition device," Med. Phys. **25**, 354–360 (1998).
[22] M. Prokop, C. Schäfer, J. W. Östmann, A. Meschede, S. Reichelt, and M. Galanski, "Optimal parameters for unsharp mask filtering in digital chest radiographs," in *CAR 1991* (Springer Verlag, Berlin, 1991), pp. 149–154.
[23] M. Stahl, T. Aach, T. M. Buzug, S. Dippel, and U. Neitzel, "Noise-resistant weak structure enhancement for digital radiography," SPIE (Medical Imaging 1999: Image Processing) **3661**, 1406–1417 (1999).
[24] J.-P. Moy, "Image quality of scintillator based x-ray electronic imagers," SPIE **3336**, 187–194 (1998).
[25] U. Schiebel, N. Conrads, N. Jung, M. Weibrecht, H. Wieczorek, T. Zaengel, M. J. Powell, I. D. French, and C. Glasse, "Fluoroscopic imaging with amorphous silicon thin-film arrays," SPIE **2163**, 129–140 (1994).